

Differing roles of CD1d2 and CD1d1 proteins in type I natural killer T cell development and function

Sundararaj, Srinivasan; Zhang, Jingjing; Krovi, S Harsha; Bedel, Romain; Tuttle, Kathryn D; Veerapen, Natacha; Besra, Gurdyal S; Khandokar, Yogesh; Praveena, T; Le Nours, Jérôme; Matsuda, Jennifer L; Rossjohn, Jamie; Gapin, Laurent

DOI:

[10.1073/pnas.1716669115](https://doi.org/10.1073/pnas.1716669115)

License:

Other (please specify with Rights Statement)

Document Version

Peer reviewed version

Citation for published version (Harvard):

Sundararaj, S, Zhang, J, Krovi, SH, Bedel, R, Tuttle, KD, Veerapen, N, Besra, GS, Khandokar, Y, Praveena, T, Le Nours, J, Matsuda, JL, Rossjohn, J & Gapin, L 2018, 'Differing roles of CD1d2 and CD1d1 proteins in type I natural killer T cell development and function', *National Academy of Sciences. Proceedings*.
<https://doi.org/10.1073/pnas.1716669115>

[Link to publication on Research at Birmingham portal](#)

Publisher Rights Statement:

Differing roles of CD1d2 and CD1d1 proteins in type I natural killer T cell development and function, Srinivasan Sundararaj, Jingjing Zhang, S. Harsha Krovi, Romain Bedel, Kathryn D. Tuttle, Natacha Veerapen, Gurdyal S. Besra, Yogesh Khandokar, T. Praveena, Jérôme Le Nours, Jennifer L. Matsuda, Jamie Rossjohn, Laurent Gapin, *Proceedings of the National Academy of Sciences* Jan 2018, 201716669; DOI: 10.1073/pnas.1716669115

Published under the PNAS license (<http://www.pnas.org/page/authors/licenses>)

General rights

Unless a licence is specified above, all rights (including copyright and moral rights) in this document are retained by the authors and/or the copyright holders. The express permission of the copyright holder must be obtained for any use of this material other than for purposes permitted by law.

- Users may freely distribute the URL that is used to identify this publication.
- Users may download and/or print one copy of the publication from the University of Birmingham research portal for the purpose of private study or non-commercial research.
- User may use extracts from the document in line with the concept of 'fair dealing' under the Copyright, Designs and Patents Act 1988 (?)
- Users may not further distribute the material nor use it for the purposes of commercial gain.

Where a licence is displayed above, please note the terms and conditions of the licence govern your use of this document.

When citing, please reference the published version.

Take down policy

While the University of Birmingham exercises care and attention in making items available there are rare occasions when an item has been uploaded in error or has been deemed to be commercially or otherwise sensitive.

If you believe that this is the case for this document, please contact UBIRA@lists.bham.ac.uk providing details and we will remove access to the work immediately and investigate.

The differing roles of CD1d2 and CD1d1 proteins in type I Natural Killer T cell development and function

Srinivasan Sundararaj^{1#}, Jingjing Zhang^{2#}, S. Harsha Krovi², Romain Bedel², Kathryn D. Tuttle², Natacha Veerapen³, Gurdyal S. Besra³, Yogesh Khandokar^{1,4}, Praveena T.^{1,4}, Jérôme Le Nours^{1,4}, Jennifer L. Matsuda⁵, Jamie Rossjohn^{1,4,6*} and Laurent Gapin^{2,5*}.

¹Infection and Immunity Program & Department of Biochemistry and Molecular Biology, Biomedicine Discovery Institute, Monash University, Clayton Victoria 3800, Australia.

²Department of Immunology and Microbiology, University of Colorado School of Medicine, Aurora, CO 80045, USA.

³School of Biosciences, University of Birmingham, Edgbaston, Birmingham, B15 2TT, UK.

⁴Australian Research Council Center of Excellence in Advanced Molecular Imaging, Monash University, Clayton, Victoria 3800, Australia.

⁵Department of Biomedical Research, National Jewish Health, Denver, CO 80206, USA.

⁶Institute of Infection and Immunity, Cardiff University, School of Medicine, Cardiff, CF14 4XN, UK.

These authors contributed equally to this work.

* These authors jointly directed this work.

Correspondence should be addressed to Dr. Laurent Gapin (Laurent.Gapin@ucdenver.edu) or Dr. Jamie Rossjohn (jamie.rossjohn@monash.edu)

Running title: Selection of type I iNKT cells by CD1d2 molecules.

Summary

Natural Killer T cells are selected by CD1d molecules in the thymus. Sundararaj et al. show that the two murine CD1d isoforms differently present lipid antigens, potentially affecting the development and TCR repertoire of NKT cells.

Abstract

Major histocompatibility complex class I-like CD1 molecules have evolved to present lipid-based antigens to T cells. Differences in the antigen-binding clefts of the CD1 family members determine the conformation and size of the lipids that are presented, although the factors that shape CD1 diversity remain unclear. In mice, two homologous genes, CD1D1 and CD1D2, encode the CD1d protein, which is essential to the development and function of Natural Killer T (NKT) cells. However, it remains unclear whether both CD1d isoforms are equivalent in their antigen presentation capacity and functions. Here, we report that CD1d2 molecules are expressed in the thymus of some mouse strains where they select functional type I NKT cells. Intriguingly, the TCR repertoire and phenotype of CD1d2-selected type I iNKT cells in CD1D1^{-/-} mice differed from CD1d1-selected iNKT cells. The structures of CD1d2 in complex with endogenous lipids and a truncated acyl chain analogue of α -galactosylceramide revealed that its A'-pocket was restricted in size compared to CD1d1. Accordingly, CD1d2 molecules could not present glycolipid antigens with long acyl chains efficiently, favoring the presentation of short acyl chains antigens. These results indicate that the two CD1d molecules present different sets of self-antigen(s) in the mouse thymus, thereby impacting the development of iNKT cells.

\body

Introduction

CD1 molecules are glycoproteins that adopt a major histocompatibility complex (MHC) class I-like structure (1). In contrast to the polymorphic MHC molecules that present peptides, CD1 molecules exhibit limited polymorphism and are ideally suited to present lipid-based antigens (2). Based on sequence homology, function and tissue distribution, the CD1 family has been classified into three distinct groups: group I, includes CD1a, -b and -c; Group II consists of CD1d, while group III is composed of CD1e (3). The number of CD1 isoforms expressed in any given mammal varies considerably however. For example, humans express all five CD1 isoforms, rabbits lack CD1c, while mice only express the CD1d protein. However, the basis for such varied usage of genes within the CD1 locus across mammals is largely unknown, but presumably reflects important functional differences related to pathogen-driven evolutionary pressures.

Lipid antigen-loaded CD1d molecules are recognized by a population of innate-like T lymphocytes, the Natural Killer T (NKT) cells. Two broad classes of NKT cells, termed type I and type II, have been defined on the basis of TCR expression and antigen reactivity (4). Type I NKT cells (or invariant (i)NKT cells) typically express a TCR that is the product of a canonical rearrangement between the $V\alpha 14$ gene segment ($V\alpha 24$ in human) and frequently the $J\alpha 18$ gene segment, with a complementary determining region (CDR) 3α region invariant at the amino acid level (5, 6). In mice, the $V\alpha 14$ invariant chain is co-expressed with a limited set of $V\beta$ chains, predominantly $V\beta 8.2$, $V\beta 7$ and $V\beta 2$, with variable CDR 3β loop sequences (7). Essentially all of these cells are responsive to the prototypical antigen α -galactosylceramide (α GC) when presented by CD1d molecules, irrespective of their TCR β repertoire diversity (8–10). How variation in CD1d itself impacts on type I NKT cell repertoire and function remains unclear however.

Upon antigenic stimulation, type I NKT cells respond rapidly by producing Th1, Th2, and Th17 cytokines, and can also be cytotoxic (11, 12). Type I NKT cells can be activated by bacterial ligands, and sense changes in host lipid metabolism through recognition of transiently expressed endogenous lipids (13–15). Chronic stimulation by these “autoantigens” leads some type I NKT cells to produce cytokines at steady state, which in turn, influences the development and activation of surrounding cells (16, 17). Thus, their unique properties establish type I NKT cells as important regulators of immune responses and tissue homeostasis (18).

In mice, two genes encoding the CD1d isoform have been identified, *CD1D1* and *CD1D2*. These two genes are located on chromosome 3 and are about 9 Kb apart, arranged in opposite transcriptional orientation (19). The two genes share 95% sequence homology with each other, and are likely the product of gene duplication (2, 20). Mouse CD1d molecules are expressed primarily by cells of the hematopoietic lineage, including B and T cells, macrophages and dendritic cells (21, 22). At the transcriptional level, *CD1D1* is expressed at higher levels than *CD1D2* in all tissues tested, except in the thymus where the mRNA levels appear to be equal for both genes (19). Of the 17 amino acid differences between CD1d1 and CD1d2 proteins, nine occur within the antigen-binding cleft, which includes a Cys168 → Trp168 mutation. The cysteine 168 residue participates in an intradomain disulfide bond that is highly conserved in classical and non-classical MHC I molecules (1, 19, 23), which is thought to be critical for the folding of MHC-I (24, 25). The impact of this mutation on CD1d2 structure and function is unknown.

The development of type I iNKT cells requires expression of CD1d by cortical thymocytes (26) and is impaired in mice lacking CD1d expression. Interestingly, while some targeting strategies led to the disruption of both *CD1D* genes (27, 28) one particular strain of *CD1D*-deficient mice, which was generated using embryonic stem cells of 129/Sv origin and has been largely distributed in the scientific community and used in multiple studies, only disrupted the *CD1D1* gene (29). Furthermore, sequencing of the *CD1D2* gene from C57BL/6 mice revealed a frameshift mutation at the beginning of the fourth exon encoding the α 3 domain thereby abolishing CD1d2 protein expression in this strain (22). Altogether, these results contributed to the assumption that CD1d2 molecules do not play any role in the development of type I NKT cells. Earlier studies that identified type I iNKT cells using co-staining for TCR β chains and the NK1.1 marker, concurred with this notion (30). However, it remains unknown whether the *CD1D2* gene is mutated in other strains of mice and whether its gene product might play a role in the selection and function of iNKT cells.

Here we report that CD1d2 molecules are expressed in the thymus of *CD1D1*^{-/-} deficient mice (29), where they select functional type I NKT cells. High throughput sequencing of *CD1D* gene transcripts from the thymus of BALB/c mice showed a transcript ratio of *CD1D1:CD1D2* close to 1:1, supporting the possibility for a role of CD1d2 in shaping the development of iNKT cells. The CD1d2 crystal structures revealed that CD1d2 adopt an overall architecture similar to CD1d1 and that the Cys168Trp mutation does not collapse the antigen-binding groove. However, the CD1d2 A' pocket was markedly restricted in size, thereby favoring the loading of lipid antigens with shorter acyl chain length, as shown by the structure of CD1d in complex with a truncated acyl chain (C10) analogue of α -GC. Collectively, our results demonstrate that CD1d2 is expressed in the thymus of some mouse

strains, where it likely presents a different repertoire of self-antigens than CD1d1 and thereby can impact on the selection of iNKT cells and their function.

Results

V α 14-J α 18 TCR usage in conventional CD4⁺ and CD8⁺ T cells from *CD1D1*^{-/-} mice. We wanted to determine the frequency of the V α 14-J α 18 rearrangement within conventional CD4⁺ and CD8⁺ TCR β ⁺ T cells. To ensure that CD4⁺ and CD8⁺ cell populations would be devoid of any potentially contaminating iNKT cells, we sorted cells from the spleens of C57BL/6 *CD1D1*^{-/-} TCR α ^{+/-} mice by flow cytometry. The frequency of gene usage was measured by qPCR and normalized to the levels found in PBS57-CD1d tetramer⁺ TCR β ⁺ cells sorted from the spleen of *CD1D1*^{+/-} TCR α ^{+/-} mice. The strategy of amplification is depicted in Sup. Fig 1. As seen in Fig 1A, 2-3% of conventional T cells use the V α 14 gene segment. Conventional splenic CD8⁺ T cells that use the V α 14 gene segment appear to only very rarely rearrange with the J α 18 gene segment, as revealed by the use of a J α 18-specific probe. Surprisingly, the situation appeared different for CD4⁺ T cells, where the results suggested that all V α 14 segments were rearranged with J α 18, like in iNKT cells. Sequencing of the PCR product showed that it corresponded to the canonical V α 14-J α 18 iNKT rearrangement (not shown). These perplexing results suggested that within the CD4⁺ T cells derived from *CD1D1*-deficient mice, V α 14 might have preferentially rearranged with J α 18, contradicting previous findings showing that V α 14 can rearrange with all J α segments (31, 32). An alternative explanation could be provided if some residual iNKT cells were still present in the sample of the sorted CD4⁺ T cells from *CD1D1*^{-/-} TCR α ^{+/-} mice. Indeed, upon careful flow cytometry analysis involving the acquisition of several millions of events, we clearly detected a population of PBS57-CD1d1 tetramer⁺ cells in the thymus, spleen and liver of *CD1D1*^{-/-} mice (Fig. 1B). This population was absent from the organs of *CD1D1/CD1D2*^{-/-} mice and greatly decreased in J α 18^{-/-} mice, which lack the invariant *Traj18* gene segment (33, 34). The few cells that were labeled in J α 18^{-/-} likely correspond to the atypical iNKT cells previously identified in that strain (34, 35). These results contrast with previous experiments that examined the presence of NKT cells in *CD1D1*^{-/-} mice using TCR β ⁺ and NK1.1⁺ co-staining and concluded that CD1d2 expression could not rescue NKT cell development (30). Instead, our results demonstrate that although the proportion of iNKT cells in *CD1D1*^{-/-} mice is only 1-4% of the iNKT cells found in the organs of C57BL/6 (B6) mice (Fig 1C), *CD1D1*^{-/-} mice should not be considered as iNKT cell-deficient and that CD1d2 molecules can potentially select for iNKT cells.

The *CD1D2* sequence from *CD1D1*^{-/-} mice and the wildtype BALB/c strain is functional. B6 mice harbor a point mutation in exon 4 of *CD1D2*, which encodes the α_3 domain (22). This frameshift mutation introduces a stop codon, abolishing surface expression of the molecule. In the 129/sv strain, however, *CD1D2* does not contain this mutation (22). To confirm that *CD1D2* in the *CD1D1*^{-/-} mice (29) is not the pseudogene found in the B6 mice, we designed primers that span part of exon 4 and

the adjoining intronic area. Genomic DNA from *CD1D1*^{-/-} mice, B6 and another wildtype strain, BALB/c, was purified and used for amplification of the exon 4 fragment. Sequencing results confirmed that whereas the B6-derived sequence contains a stop codon in exon 4, BALB/c and the 129/Sv-derived *CD1D1*^{-/-} mice had a functional *CD1D2* sequence (not shown). These results demonstrate that no crossover of the CD1 locus ever occurred during the backcross of the *CD1D1*^{-/-} to B6 mice and that the CD1 locus is of 129/sv origin in these mice. Furthermore, these results suggest that CD1d2 molecules have the potential to be expressed in BALB/c mice.

CD1d2 protein is expressed in the thymus but not the periphery of *CD1D1*^{-/-} mice. Because no serological reagent currently exists to discriminate CD1d1 from CD1d2 proteins, we first examined CD1d2 expression on cells derived from B6 *CD1D1*^{-/-} mice. Controls were provided by staining cells from double deficient *CD1D1/CD1D2* mice (27, 30) and heterozygous *CD1D1*^{+/-} mice generated by crossing *CD1D1*^{-/-} mice with B6 mice. In this latter strain, the CD1d protein levels represent the combined gene activity of a single copy of *CD1D1* B6 allele (because *CD1D2* is mutated in B6) and a single copy of the functional *CD1D2* allele from the KO mice (because *CD1D1* has been knocked out in these mice and the *CD1D2* allele is of 129/Sv origin). As seen in Fig. 2, we observed a low level of CD1d expression in the thymus of *CD1D1*^{-/-} mice, attributable to CD1d2 expression (Fig 2A). In particular, while *CD1D1*^{+/-} thymocytes displayed haploinsufficient patterns, expressing half of the amount of CD1d found on thymocytes from wildtype mice (as measured by gMFI), the *CD1D1*^{-/-} thymocytes expressed only 1/25 of the level expressed in wildtype mice (Fig 2C). Interestingly, this expression was limited to the thymus, in agreement with previous results (30). In the periphery, we observed no protein expression of CD1d2 on whole splenocytes or individual splenic populations (Fig 2B and D).

Early experiments using RNase protection assays suggested that *CD1D2*-encoding transcripts were equally abundant compared to *CD1D1* transcripts in BALB/c thymocytes (19). To verify these findings, we generated cDNA from B6 and BALB/c DP thymocytes and amplified a portion of exon 2 using primers targeting identical sequences between *CD1D1* and *CD1D2* genes. This segment of DNA, however, contains eight nucleotide polymorphisms between the two genes. PCR products were sequenced using high throughput sequencing and the relative expression of *CD1D1* and *CD1D2* transcripts were determined in each strain. The transcript ratio of *CD1D1* to *CD1D2* was overwhelmingly skewed towards *CD1D1* in B6, with an expression ratio close to 5:1. This likely reflects the degradation of *CD1D2*-encoding mRNA due to non-sense mediated mRNA decay (36). In BALB/c, however, the ratio of *CD1D1:CD1D2* is close to 1:1 (Fig 2E). Altogether, these results demonstrate that CD1d2 molecules can be expressed in the thymus of mice with a functional *CD1D2* gene.

Development and repertoire of CD1d2-selected iNKT cells. We enriched PBS57-CD1d1⁺ cells from the thymus of B6 and *CD1D1*^{-/-} mice using magnetic beads and analyzed the maturation of iNKT cells using the cell surface markers CD44 and NK1.1 to follow their maturation progress from stage 1-3 (37, 38). CD1d2-selected iNKT cells in *CD1D1*^{-/-} mice appeared less mature compared to CD1d1-selected iNKT cells from B6 mice (Fig 3A). Indeed, the majority of iNKT cells in the *CD1D1*^{-/-} mice were of the more immature stage 1 (CD44⁺NK1.1⁻) or stage 2 (CD44⁺NK1.1⁻) phenotype, as compared to wildtype where about 80% of cells are the most mature stage 3 (CD44⁺NK1.1⁺) phenotype (Fig. 3C). However, the absolute number of iNKT stages detected in *CD1D1*^{-/-} thymi was significantly lower than that observed in control thymi, due to reduced total iNKT cell numbers in the *CD1D1*^{-/-} mice. Because analysis of iNKT cells by staging is insufficient, as populations within each stage are heterogeneous (16, 39), we also characterized the CD1d2-selected iNKT cells by their expression of the transcription factors PLZF, ROR γ t and Tbet to define terminally differentiated effector cells. Compared to the iNKT subset makeup found in the B6 thymus, iNKT cells in the thymus of *CD1D1*^{-/-} mice showed a trending increase in the NKT2 (PLZF^{hi}, Tbet^{lo}, ROR γ t^{lo}) and NKT17 (PLZF^{mid}, Tbet^{lo}, ROR γ t^{hi}) populations and a concomitant decrease in NKT1 (PLZF^{lo}, Tbet^{hi}, ROR γ t^{lo}) cells (Fig 3B and C). Interestingly, although the vast majority of the CD1d2-selected iNKT cells are of the NKT1 phenotype (ie. PLZF^{lo} Tbet^{hi}), these cells are mostly NK1.1⁻ and lack expression of the NK receptors Ly49C/I, in striking contrast with the same population of iNKT1 cells in B6 mice (Fig 3B). This might have contributed to their lack of detection in previous studies (30).

Next, we examined the V β repertoire expressed by iNKT cells selected on CD1d1 in B6 mice or on CD1d2 in *CD1D1*^{-/-} mice by flow cytometry. Similar to what has been reported previously for the CD1d1-selected iNKT repertoire (40, 41), CD1d2-selected iNKT cells were enriched for V β 8 and V β 7⁺ cells compared to conventional T cells (data not shown). However, a small but consistent increase in the proportion of cells using the V β 8 gene segment, concomitant to a reduction in V β 7 gene usage, was observed for CD1d2-selected iNKT cells compared to CD1d1-selected iNKT cells (Fig 3D). To further compare the TCR repertoires of CD1d1-selected and CD1d2-selected iNKT cells, we sorted PBS57-CD1d1 tetramer⁺ cells from the thymi of 2 C57BL/6 mice and 30+ pooled *CD1D1*^{-/-} thymi. Total RNA was extracted and cDNA was synthesized. We amplified V β 8.1/8.2 rearrangements using specific V β 8.1/2 and C β primers and the PCR fragments were sequenced using next generation sequencing. Figure 3E represent a visual depiction of all the sequence found in the B6 and *CD1D1*^{-/-} V β 8⁺ iNKT repertoires, where every dot represents a unique CDR3 β sequence, the size of the dot represents how many times this sequence was found, and the color represents which J β was used. As expected, CD1d1-selected iNKT cells expressed a polyclonal repertoire with no overrepresentation of any particular sequence (42). Although the CD1d2-selected iNKT cell repertoire was also polyclonal, it appeared to be much more limited, with fewer clones and fewer J β s represented. In fact,

when comparing the overlap between the two repertoires, we observed that only 16% of the sequences from *CD1D1*^{-/-} iNKT cells were contained within the B6 repertoire. Thus, the majority of V β 8.1/8.2 TCR sequences found in the iNKT cells from *CD1D1*^{-/-} appear unique to these iNKT cells. To further explore the antigen reactivity of CD1d1 vs CD1d2-selected iNKT TCR repertoires, we cloned libraries of V β 8.1/8.2 TCR sequences into retroviral plasmids. We then transduced a TCR-negative T hybridoma with the V α 14-J α 18 TCR α chain and the two different V β 8 libraries derived from either B6 or *CD1D1*^{-/-} iNKT cells. The hybridoma was further transduced with a NFAT-GFP construct, allowing for measurement of TCR stimulation on a per cell basis. Hybridomas expressing V β 8 TCR repertoires derived from B6 or *CD1D1*^{-/-} mice were cultivated overnight in the presence of the CHB lymphoma that had been previously transfected (or not) with CD1d1 or CD1d2 expressing constructs. As seen in figure 6C, about 2% of the hybridoma expressing the B6 iNKT cell repertoire expressed GFP upon stimulation by CD1d-expressing APCs. The proportion of autoreactive cells was increased to 4-5% of the cells when the repertoire derived from *CD1D1*^{-/-} iNKT cells was interrogated in a similar fashion (Fig 3F). Cell sorting of these GFP⁺ cells and subsequent re-stimulation with CD1d-expressing APCs demonstrated the autoreactivity of these cells towards CD1d-expressing APCs (data not shown). Altogether, these data suggest that the TCR repertoire of iNKT cells found in *CD1D1*^{-/-} mice is more autoreactive than the TCR repertoire expressed by B6-derived iNKT cells. This might be due to the nature of the CD1d2 molecules themselves, alterations in the self-lipid repertoire and/or their low levels of expression in the thymus of *CD1D1*^{-/-} mice (Fig 2).

CD1d2-selected iNKT cells are functional. To test whether CD1d2-selected iNKT cells were functional *in vivo*, we injected 2 μ g of the prototypic antigen α GC, which has a 26 carbon long fatty acid chain, intravenously to B6 and *CD1D1*^{-/-} mice and harvested livers from the animals 90 minutes later to interrogate IL-4 and IFN- γ production within iNKT cells (41). Unlike B6 controls, in which 90% of iNKT cells were activated as detected by IFN- γ intracellular cytokine staining, no *CD1D1*^{-/-}-derived iNKT cells were responsive to injected antigen, resembling PBS injected controls (data not shown). These results probably reflect the absence of the CD1d molecule expression in the peripheral tissues required to present the antigen. However, iNKT cells can also be activated in a TCR independent manner in response to inflammatory cytokines secreted by activated antigen presenting cells (43, 44). Therefore, we injected 40 μ g of LPS or PBS control to B6 or *CD1D1*^{-/-} mice and harvested their livers 7 hours after injection. Cells were stained intracellularly for IFN γ directly *ex vivo* without further stimulation and/or addition of brefeldin A. Although the activation of iNKT cells through LPS is less robust than through TCR engagement by the α GC/CD1d complex, the results clearly demonstrated that both CD1d1-selected as well as CD1d2-selected iNKT cells could produce IFN γ under these conditions (Fig 3G and H). These results demonstrate that CD1d2-selected iNKT cells are functional

and capable of secreting cytokines upon stimulation. Furthermore, these results support the idea that the maintenance of iNKT cell effector function is TCR independent and does not require tonic signaling mediated by CD1d molecules.

Overall architecture of CD1d2. To gain insight into the detailed architecture of the CD1d2 molecule, we expressed and purified CD1d2 from the supernatant of insect cells and subsequently determined its structure. CD1d2 adopted a standard MHC-I fold, like CD1d1 (Fig. 4 and supplementary table 1). Similar to the overall architecture of other CD1 molecules (45–48), the α 1- and α 2-helices are positioned atop of a six anti-parallel β -strands platform to form a deep hydrophobic antigen-binding groove ($\sim 1300 \text{ \AA}^3$) that accommodates lipid-based antigens (Fig. 4A). Following the nomenclature adopted for mouse CD1d1 (3), the antigen-binding cleft is composed of two distinct A'- and F'-pockets (Figs. 4A & 4B) that differ in size and architecture. The contour of the A'-portal ($\sim 550 \text{ \AA}^3$) is delineated by a number of bulky hydrophobic residues (W40, F70, Y73, F77, F116 and W168) with residues Y73 and F77 separating the A'- from the F'-pocket (Fig. 4B). The F'-pocket (750 \AA^3) is shaped by an extensive network of hydrophobic residues. Here, residues L100, V118, F120, A125, F128 and L143 form the floor of the pocket whilst a number of key hydrophobic residues from the α 1- and α 2-helices (Y73, F77, I81, L84, V85, M88, W142, L143, P146, I147, L150 and T156) define the overall shape of the F'-pocket (Fig. 4B, right panel).

The CD1d2 crystal structure also revealed clear separate unaccounted and continuous electron density within the A'- and F'-portals to protrude out of the binding cleft (Sup. Fig 2). This density suggested the presence of an endogenous bound lipid containing a head group that was acquired from the Hi5 insect cells during the recombinant expression of CD1d2. Although the precise identity of the endogenous ligand is undetermined, we modeled in the unbiased electron density the common self-membrane phospholipid, phosphatidic acid (PA). This enabled us to evaluate the approximate length of the acyl chains that the endogenous lipid may contain. PA consisting of two acyl chains composed of 10 and 18 carbons could accommodate the continuous electron density that was visible in the A'- and F'-pockets, respectively (Sup. Fig 2).

To formally demonstrate that CD1d2 present lipid antigens of shorter acyl chain length, we conducted lipid loading experiments with a truncated analogue of α GC in which the acyl chain was 10 carbon atoms in length (α GC (C10)). While we could not load recombinant CD1d2 with α GC, the α GC (C10) form readily complexed with CD1d2. We then subsequently determined the structure of CD1d2- α GC (C10) (Supplementary Table 1), in which the C10 acyl chain was clearly observed within the A'-pocket of CD1d2. The structure of CD1d2- α GC (C10) was very similar to that of CD1d2 bound to

endogenous lipids, and the mode of α GC (C10) presentation by CD1d2 was very similar to that of CD1d1- α GC. Accordingly, CD1d2 can present α GC (C10) in a manner analogous to CD1d1 presentation of α -GC.

Comparison of the CD1d2 and CD1d1 crystal structures. CD1d2 and CD1d1 share high amino acid sequence identity (93%) (Sup. Fig 3), that is reflected by a very similar α 1- and α 2-domains architecture with a root mean square deviation (r.m.s.d) of 0.9 Å over 178 C α atoms (Fig. 4D). Thus, the presence of the Cys168Trp polymorphism did not lead to gross conformational changes in the CD1d2 architecture. The majority of the polymorphisms between CD1d1 and CD1d2 are evenly distributed over the α 2-helix and the six β -sheet platform, whereas the α 1-helix sequence is conserved between CD1d1 and CD1d2 (Fig. 4D and Sup. Fig. 3). Ten of these polymorphic residues are located on the molecular surface of CD1d2 (Sup. Fig. 4A). The remaining six residues (I30, T102, F116, W168 and A172 in CD1d2) are predominantly buried within the A'-pocket of CD1d2 (Fig. 4D and Sup. Fig. 4B). Interestingly, residues I30, T102, F116 and W168 are directly implicated in remodeling the overall architecture of the A'-portal relative to CD1d1 (Figs 4E and 5A, and Sup. Fig. 4B). The substitution of V30, L116 and C168 in CD1d1 by the bulkier hydrophobic I30, F116 and W168 residues in CD1d2, respectively, contribute to a reduction of the A'-pocket volume of CD1d2 by ~ 400 Å³ compared to CD1d1, and also serves to prevent the collapse of the A'-pocket due to the lack of the intermolecular disulfide bond. Here, in order to accommodate the endogenous lipid and α GC (C10), the side chain of F70 was repositioned in close vicinity of I30 and W168 (~ 4 Å distance), and consequently this triad of residues contributed to restrict the size of the A'-portal (Figs. 4E and 5A). Accordingly, the structural rearrangement incurred by these polymorphic residues may impact the overall repertoire of lipids that can be presented by CD1d2 compared to CD1d1. Modeling of longer acyl chains in the A'-pocket was sterically disfavored by the architecture of the CD1d2 groove (Figs. 5C and 5D). Indeed, the A'-pocket of CD1d2 favors the loading of shorter sized lipids than that of CD1d1, as evidenced by the CD1d2- α GC(C10) structure. In the CD1d2 A'-pocket, residues T102 and F116 also impacted the overall position of the acyl chain of the endogenous lipid (Fig. 5B). By contrast, the F'-pockets of CD1d2 and CD1d1 are highly conserved (Fig. 4D) whereby only A125 (CD1d2) was replaced by V125 (CD1d1) (Figs. 4D-E). Thus, molecular insights into the antigen-binding cleft of CD1d2 show that lipid antigens with long acyl chains are not as efficiently presented compared to CD1d1 molecules.

Differential antigen presentation by CD1d1 and CD1d2 molecules. To test the antigen presentation ability of both CD1d1 and CD1d2 molecules, we cultivated hybridoma cells expressing a library of iNKT TCRs (expressing different TCR β chains) derived from B6 thymic iNKT cells with B cell

lymphoma CHB cells expressing similar levels of either CD1d1 or CD1d2 molecules. Increasing concentrations of various antigens were added to the cultures and the percentage of GFP⁺ hybridoma cells was assessed after 18 hours. As seen in Fig 6, CD1d2-expressing CHB cells poorly stimulated the hybridomas compared to CD1d1-expressing cells when cultivated in the presence of glycolipid antigens with long acyl-chains, including the prototypical iNKT antigen α GC (C26), the α GC variant with a shorter sphingosine chain OCH9 (C24), and the *sphingomonas*-derived antigen GSL-1 (C14). In striking contrast, a version of α GC with a 10 carbon acyl chain, or the α -psychosine antigen, which lack an acyl chain (49, 50), equivalently stimulated the hybridoma when cultivated with CD1d1 or CD1d2-expressing cells. The β -anomeric form of psychosine did not stimulate the hybridoma when cultivated with either APCs. CHB cells expressing CD1d1 molecules with the Cys168 \rightarrow Trp168 mutation were also poor presenter of α GC (C26) but could present α GC (C10) as efficiently as wildtype CD1d1 molecules (Fig. 6). Altogether, these results suggest that CD1d2 molecules are poor presenter of long-acyl chain glycolipid antigens but can present certain antigens with short acyl-chains as efficiently as CD1d1 molecules. These results demonstrate that both CD1d molecules in mice are not equivalent and can selectively present different lipid antigens to iNKT cells.

CD1d2- α GC-C10 tetramer⁺ cells. Having established that CD1d2 molecules preferentially present glycolipid antigens with short-acyl chains, we loaded soluble CD1d2 monomers with α GC (C10) and generated CD1d2 tetramers. Thymocytes from BALB/c, B6, *CD1D1*^{-/-} and *J α 18*^{-/-} mice were independently stained using the PBS57-CD1d1 or the α GC(C10)-CD1d2 tetramers (Fig. 7A). The percentage of cells stained in each thymus was essentially identical between both tetramers, although α GC(C10)-CD1d2 tetramers stained with lower intensity compared with PBS57-CD1d1 tetramers. Co-staining with saturating concentrations of CD1d1 and CD1d2 tetramers loaded with PBS57 or α GC(C10), respectively, were initially unsuccessful because no CD1d2 signal was detected in these instances (data not shown). However, sequential staining with the two tetramers could be achieved if CD1d2 tetramers were used first. Using this strategy, we did not detect a significant population of α GC(C10)-CD1d2-specific cells (Fig. 7B). Instead, a fraction of iNKT cells was stained with both tetramers, while some PBS57-CD1d1 tetramer⁺ cells were not labeled with the α GC(C10)-CD1d2 tetramer. Interestingly, cells labeled with the α GC(C10)-CD1d2 tetramer expressed the highest levels of TCR on their surface (Fig. 7B), suggesting that the α GC(C10)-CD1d2 binds only to the highest avidity iNKT TCRs.

Discussion

Peptide-presenting major histocompatibility molecules are encoded by the most polymorphic genes in the genome. Most of this polymorphism involves residues that are lining up the antigen-binding groove

of MHC molecules (51). At the population level, this polymorphism provides various possible binding solutions to the myriad of antigenic peptides that need to be presented for immunosurveillance by T cells. By contrast, lipid-binding CD1 molecules are essentially monomorphic. Instead diversity of lipid antigen presentation is achieved through the use of multiple genes, each encoding a different CD1 molecule with a unique antigen-binding groove adapted to present structurally diverse classes of lipids (2, 52). The number and complexity of CD1-encoding genes varies greatly between species. For example, the microbat possesses a total of 26 CD1-encoding genes while the dolphin has only 1 (53). The functional consequence of expressing multiple isoforms presumably reflects pathogen-driven evolutionary pressure. The mouse genome contains two genes, *CD1D1* and *CD1D2*, which encode for the CD1d isoform. A collection of observations has contributed to the misleading idea that *CD1D2* might not play any relevant role in the biology of lipid-reactive T cells. First, the ubiquitously used C57BL/6 mice contain a frame-shift mutation in *CD1D2*, which prevents its expression (22). Second, a highly conserved cysteine residue that form a disulfide bridge between the α 2 helix and β -sheet floor of the antigen binding groove of MHC class I molecules is replaced by a tryptophan in CD1d2 molecules, leading to the speculation that the protein may not adopt the proper MHC folding (19, 25). Finally, it was reported that CD1d2 molecules could not compensate for the development of NKT cells in *CD1D1*-deficient mice (30). By contrast, we show that in the 129/Sv and BALB/c mouse strains, the *CD1D2* gene is functional and in BALB/c mice is expressed equivalently to the *CD1D1* gene at the mRNA level in the thymus. Analysis of CD1d2 protein expression in the thymus of *CD1D1*^{-/-} mice demonstrated that the protein could be expressed in this tissue albeit at 1/25th of the levels observed in wildtype animals. It is unclear whether these results reflect the actual levels of protein expression that could be achieved in wildtype mice with a functional gene. Specifically, in both *CD1D1*-deficient strains analyzed (29, 30), the pgk-neomycin selection cassette used to select the embryonic cell line from which the mouse strains were generated remains in their genomes. At this time, the possibility that the selection cassette could have an adverse effect on *CD1D2* transcription (34) cannot be excluded. Irrespective of its low level of expression in the thymus of *CD1D1*^{-/-} mice, CD1d2 molecules are clearly capable of selecting some iNKT cells in these mice. Consequently, mice lacking only the *CD1D1* gene (29) should not be considered as NKT cell-deficient.

Interestingly, the phenotype and repertoire of the CD1d2-selected iNKT cells in *CD1D1*^{-/-} mice was not equivalent to the CD1d1-selected iNKT cells in B6 mice. The iNKT cells in the thymus of *CD1D1*^{-/-} mice were somewhat enriched for the iNKT2 and iNKT17 subsets compared to the subset composition encountered in age-matched B6 mice. Furthermore, the thymic iNKT1 subset in *CD1D1*^{-/-} mice expressed little to no NK1.1 molecules, which usually characterize this subset in B6 mice. Similarly, the V β repertoire of CD1d2-selected iNKT cells was enriched for usage of the V β 8 chain with a concomitant decrease in V β 7 usage compared to the CD1d1-selected iNKT cells. Previous

reports showed that changes in V β selection occurred in mice expressing lower or higher levels of CD1d, and reflected changes in positive and negative selection according to V β affinities for self-ligand presented by CD1d molecules (54, 55). The TCR V β domain influences the thymic selection of iNKT cells by contributing to the avidity of iNKT TCR binding to CD1d complexed with endogenous ligand(s) (8). In haplosufficient *CD1D*^{+/-} mice that express half the levels of CD1d compared to wildtype mice, V β 7⁺ iNKT cells were overrepresented with a concomitant decrease in V β 8 usage, suggesting that V β 7-containing iNKT TCRs have higher affinity for the self-ligand(s)-CD1d complexes that are responsible for the positive selection of these cells. By contrast, in *CD1D1*^{-/-} mice, the expression level of CD1d2 was only 5% of the level of CD1d observed in wildtype mice and yet we observed a preferential enrichment of V β 8⁺ iNKT cells. Sequencing of the CDR3 region of these V β 8⁺ iNKT cells demonstrated poor overlap with the repertoire of B6 V β 8⁺ iNKT cells. Furthermore, the CD1d2-selected V β 8 iNKT repertoire tended to be more autoreactive when re-expressed in an *in vitro* system. The reason(s) for these differences remains unclear. It is possible that the low level of CD1d2 expression contributed to the selection of iNKT cells expressing TCR of the highest avidity, which would otherwise be negatively selected in wildtype animals. Alternatively, the presentation of a different set of self-antigen(s) responsible for the positive selection of iNKT cells between CD1d1 and CD1d2 could contribute to these differences in repertoire and phenotype. Both possibilities are not exclusive. Future experiments aimed at manipulating the expression level of CD1d2 to match the levels observed for CD1d1 should be informative in that matter.

One aspect that determines the function of a CD1 protein is the size and shape of the antigen-binding groove. For example, human CD1b has a large antigen-binding groove that can accommodate ligands up to 80 carbon atoms in length (46). In contrast, the human CD1a isoform has a unique architecture that appears to favor “headless” antigens, with a restricted A'-pocket that prefers lipids of shorter acyl chain length (C18-C20) (47, 56). Our work resonates with the CD1a molecule in that CD1d2 favors the presentation of shorter length lipid ligands in comparison to CD1d1. Despite high homology between the two CD1d molecules, changes in amino acids at position I30, T102, F116 and especially W168, restrict the size of the A'-pocket of CD1d2. The Trp 168 blocks part of the A'-pocket so that long fatty acid chain glycolipids will not fit. In agreement with the structural data, APCs engineered to express the CD1d2 molecules or the C168W CD1d1 mutant, were poor presenters of common glycosphingolipids, including the prototypical antigen α GC, which consist of fatty acid with a length of 24-26 carbons. Interestingly, comparable observations had been previously reported whereby the equivalent cysteine residue in the bovine CD1d and the ancestral chicken CD1-2 are replaced by a tryptophan and phenylalanine, respectively (57, 58). These restricted the size of the A'-pocket of the two isoforms and reduced their capacity to bind long-chain lipid-based antigens (57, 58). By contrast, CD1d2 efficiently presented glycolipid antigens with short (<10 carbons) or no

acyl chains. Of interest, α -psychosine, which contains a single lipid chain and has been proposed to possibly play a role in the selection of iNKT cells (49), was efficiently presented by both CD1d molecules. Although the lipid portions of antigens are buried in the CD1d groove, the composition of the fatty acids, including the length, the degree of unsaturation and the presence of other modifications, strongly influences antigenic potency (59–61). As such, it is reasonable to hypothesize that the balance between the various antigen species that might be presented by either CD1d1 and/or CD1d2 in the thymus possibly affects the tuning of the iNKT TCR repertoire to different ligands.

Acknowledgments. We thank members of our laboratories for thoughtful discussions and critical comments on the manuscript; Chyung-Ru Wang for the *CD1D1D2*^{-/-} mice used in this study; Paul B. Savage and Luc Teyton for the α and β -psychosine antigens; the National Jewish Health flow cytometry facility, the Mucosal and Vaccine Research Colorado Flow Core, and the University of Colorado flow cytometry shared resource facility for assistance with cell sorting; the Center for Genes, Environment, and Health at National Jewish Health for sequencing and the National Institutes of Health core facility for CD1d tetramers. We thank the staff at the National Synchrotron for assistance with data collection and the staff at the Monash Macromolecular crystallization facility. This work was supported by National Institutes of Health Grants AI121761 and AI124076 (to L.G.); The American Association for Immunologists Careers in Immunology Fellowship (to L.G.); The Cancer Center Support Grant P30CA046934; the National Health and Medical Research Council (NHMRC), the Worldwide Cancer Research grant 16-1106 (to J. R.) and ARC Future Fellowship to (J. LN).

Author contributions L. G., J. R., J. Z., J. L. N. wrote the manuscript and designed figures. L. G., J. R., J. Z., S. H. K., J. LN. designed experiments. S. S., J. Z., R. B., K. T., S. H. K., J. L. N., Y.K., P.T. conducted experiments. S. S., J. Z., R. B., K. T., S. H. K., J. L. N., Y.K., P.T. acquired data. J. Z., S. S., J. LN., J. R., L. G. analyzed and interpreted data. N. V., G. S. B. provided invaluable reagents. J. Z., S. S., J. LN., L. G. and J. R. edited the manuscript. All authors approved final manuscript.

Figure legends

Figure 1. Frequency of V α 14 usage and V α 14-J α 18 rearrangement usage amongst CD4⁺ and CD8⁺ T cells purified from the spleen of *CD1D1*^{-/-} mice and iNKT cells in *CD1D1*^{-/-} mice. (A) Relative frequency usage V α 14 and V α 14-J α 18 usage in CD4⁺ and CD8⁺ T cells from *CD1D1*^{-/-} mice. The frequency was normalized to the amount of the various PCR products found in iNKT cells sorted from the spleen of *CD1D1*^{+/-} TCR α ^{+/-} mice that was set at 100%. Results are shown as mean \pm SD. (B) Cells from the thymus, spleen and liver of 6–8 week old C57BL/6, *CD1D1*^{-/-}, *CD1D1D2*^{-/-}, and J α 18^{-/-} mice were stained with CD1d1 tetramers loaded with PBS57 (PBS57-CD1d) and TCR β mAbs and analyzed by flow cytometry (data representative of n \geq 3 per group across two experiments). The percentage of iNKT cells in each sample is shown. (C) Summary of the data shown in (B) with percentage of iNKT cells in thymus, spleen and liver of 6–8 week old C57BL/6, *CD1D1*^{-/-}, *CD1D1D2*^{-/-}, and J α 18^{-/-} mice. *p < 0.05; **p < 0.01; ***p < 0.001; ****p < 0.0001; ns, not significant.

Figure 2. *CD1D1*^{-/-} mice express low amounts of CD1d molecules on the surface of hematopoietic cells of the thymus, but not the periphery. (A) Flow cytometric analysis of CD1d levels of thymic DP (CD4⁺CD8⁺), CD4, and CD8 subsets from C57BL/6 (black), *CD1D1*^{+/-} (grey), *CD1D1*^{-/-} (red) and *CD1D1D2*^{-/-} (blue) mice. (B) Flow cytometry analysis of CD1d levels of spleen T and B subsets derived from the aforementioned mouse strains. (C) Bars represent the relative gMFI of CD1d expression on total thymocytes, normalized to C57BL/6. Bars depict mean \pm SEM of at least three mice per group across at least two experiments. ***P < 0.001 by student t-test. (D) Bars represent the relative gMFI of CD1d expression on total splenocytes, normalized to C57BL/6. Bars depict mean \pm SEM of at least three mice per strain across at least two experiments. (E) Ratio of *CD1D1/CD1D2*-encoding transcripts in the thymus of B6 and BALB/c mice. Primers containing specific Ion Torrent tags were designed against segments identical in exon 2 of *CD1D1* and *CD1D2* genes. CD69⁻CD4⁺CD8⁺ pre-selection DP thymocytes were sorted from 3 independent B6 and 3 independent BALB/c mice, mRNA was extracted and transformed into cDNA. CD1d exon sequence was amplified and PCR products were sequenced using high throughput sequencing. Transcript identity was determined based on 8 nucleotides polymorphism (depicted as *) that exists between the two genes in this exon. The ratio of CD1D1 and CD1D2 mRNA expression was significantly different between the two strains (p < 0.0001).

Figure 3. Development and repertoire of CD1d2-selected iNKT cells. PBS57-CD1d1 tetramer reactive thymocytes were enriched from C57BL/6 and pooled *CD1D1*^{-/-} thymi (\geq 5 mice per sample) using MACS beads. Enriched cells were stained with indicated markers and assessed by flow

cytometry to characterize specific stages of iNKT-cell development (A) (data representative of $n \geq 3$ per group) or functional subsets of iNKT cells as defined by the expression of the transcription factors PLZF, RoR γ t and Tbet (B). (C) Graphs depict mean \pm SEM of (A) and (B). * $p < 0.05$; ** $p < 0.01$; *** $p < 0.001$; **** $p < 0.0001$; ns, not significant. (D) PBS57-CD1d1 tetramer reactive thymocytes were enriched by MACS beads from individual B6 or pooled *CD1D1*^{-/-} thymi (≥ 5 mice per sample). Enriched cells were stained with PBS57-CD1d1 tetramers, TCR β , V β 8, V β 7, V β 2 mAbs and assessed by flow cytometry to characterize V β usage (data representative of $n \geq 3$ samples per group). Bars depict mean \pm SEM of percent of iNKT cells expressing each V β . * $p < 0.05$; ** $p < 0.01$; *** $p < 0.001$; **** $p < 0.0001$; ns, not significant. (E) Visual representation of V β 8 CDR3 sequences from sorted iNKT cell of B6 (left) and *CD1D1*^{-/-} (right) mice. Each CDR3 sequence is represented by a dot with the size of the dot proportional to the number of times this CDR3 sequence was found with the sample and each J β is represented by a color. V β 8 rearrangements were amplified by PCR with a V-specific primer and a C-specific reverse primer followed by high-throughput sequencing using the Ion Torrent platform. Sequence analysis was performed with in-house software, and gene identity was assigned on the basis of sequence alignment with published sequences (International ImMunoGeneTics Information System). (F) V β 8 rearrangements from B6 and *CD1D1*^{-/-} iNKT cells were amplified and cloned into retroviral plasmids. Retroviruses were produced and used to transduced V α 14-expressing hybridoma. Hybridoma were sorted for similar TCR expression and transduced with NFAT-GFP reporting construct. Antigen presentation assay using the B cell lymphoma cells CHB transfected or not with *CD1D1* or *CD1D2* expressing constructs were performed. The percentage of GFP⁺ hybridoma cells from triplicate cultures was recorded using flow cytometry after 18h of cultures and quantified. * $p < 0.05$; ** $p < 0.01$; *** $p < 0.001$; **** $p < 0.0001$ by 2-way ANOVA. Results are representative of three independent experiments. (G) Intracellular IFN γ expression of liver iNKT cells 7 hours after LPS injection. iNKT cells were identified using PBS57-CD1d1 tetramer and TCR β mAbs and stained intracellularly for IFN γ . Plots are representative of at least 3 mice per group. (H) Bars depict mean \pm SEM of percent of responding iNKT cells within each strain or condition. * $P < 0.05$; ** $P < 0.01$; *** $P < 0.001$; **** $P < 0.0001$; ns, not significant.

Figure 4. CD1d2 crystal structure. (A) Cartoon representation of the CD1d2 crystal structure. CD1d2 and β 2m are colored in grey and light orange, respectively. (B) Close-up views of the A'- (left panel) and F'-pockets (right panel) of CD1d2. Both pockets are colored in pale green and shown as surface representation. (C) Left panel, unbiased Fo-Fc electron density map (in magenta) contoured at 2.0σ level of the α GC (C10) lipid Ag. Right panel, 2Fo-Fc electron density map (in marine) contoured at 0.8σ level of the α GC (C10) lipid Ag. The lipid Ag is shown as black sticks. For clarity, only the α 1- and α 2- helices of CD1d2 are colored in light grey and shown as cartoon representation. (D)

Superimposition of the α 1- and α 2-domains of the crystal structures of CD1d2 (in grey) and CD1d1 (PDB code: 1CD1) (in light blue) (45). The polymorphic residues between CD1d2 and CD1d1 are shown as sticks. For clarity, only the residues located inside the binding groove are shown. (E) Surface representation of the binding pocket of CD1d1 (in pale yellow) shown in two orientations. A superimposition of the α 1- and α 2-domains of the CD1d2 (in grey) and CD1d1 (in light blue) is also shown.

Figure 5. Structural comparison between CD1d1 and CD1d2. (A) Close-up view of a superposition of the A'-pockets of CD1d1 and CD1d2 shown in yellow and light green, respectively. (B) (C) Superimposition of CD1d-phosphatidylcholine (in orange) (PDB code: 1ZHN) (62), CD1d-dioleoyl-phosphatidic acid (in teal) (PDB code: 4MX7), CD1d- α GC (C25) (in violet) (PDB code: 3HE6) (9) and CD1d2- α GC (C10) (in black). (D) Close-up view of (A). In panels A-D, the α 1- and α 2-domains of the CD1d2 (in grey) and CD1d1 (PDB code: 1ZHN) (in light blue) are shown.

Figure 6. Differential antigen presentation by CD1d1 and CD1d2 molecules. Hybridoma expressing $V\beta 8^+$ iNKT TCRs derived from C57BL/6 iNKT cells were cultivated for 18 hours with CHB cells stably transfected with either *CD1D1* (black), *CD1D2* (red) or the *CD1D1* mutant in which the cysteine 168 was replaced by a tryptophan (green) and the indicated glycolipid antigens. Graphs depict the percentage of GFP⁺ hybridoma as a function of antigen concentration. Data represent the mean of duplicates for each condition and are representative of 3 independent experiments.

Figure 7. α GC(C10)-CD1d2 tetramer staining. (A) Thymocytes from BALB/c, C57BL/6, *CD1D1*^{-/-} and *J α 18*^{-/-} mice were stained with CD1d1 tetramers loaded (or not) with PBS57 or CD1d2 tetramers loaded (or not) with α GC (C10) and TCR β mAbs. The percentage of tetramer⁺ is shown. Data are representative of two independent experiments. (B) Thymocytes from the aforementioned mouse strains were first stained with α GC (C10)-CD1d2 tetramers, washed and subsequently stained with PBS57-CD1d1 tetramers. Data are representative of three independent experiments. Simultaneous staining with both tetramers did not allow for the detection of the fluorophore associated with the CD1d2 tetramer.

Materials and Methods

Mice. The *CD1D1*^{-/-} (29), *CD1D1*^{-/-} *CD1D2*^{-/-} (27) and *J α 18(neo)* (33) mice have been described previously and were backcrossed >10 times on the C57BL/6 background. C57BL/6 and BALB/c were purchased from Jackson Laboratories. All mice were used between 6 to 12 weeks and were age

matched for each experiment. All mice were raised in a specific pathogen-free environment at the Biology Resource Center in National Jewish Health and the Office of Laboratory Animal Research at UCD. All animal procedures were approved by the NJH (AS2780-10-16) and UCD (B-64314(05)1E) Institutional Animal Care and Use Committee and were carried out in accordance with the approved guidelines.

Lymphocyte Isolation. Single cell suspensions were prepared from the thymus, spleen, and liver by manual disruption using syringe plunger. The liver was perfused with PBS then cut into small pieces, disrupted with a syringe plunger, and liver lymphocytes were isolated by centrifugation using a 33% (vol/vol) Percoll gradient (GE Healthcare).

High-Throughput Sequencing. CD69⁻CD4⁺CD8⁺ pre-selection double positive thymocytes were sorted by flow cytometry and washed twice in ice-cold PBS. Total RNA was extracted using the RNeasy Mini Kit (Qiagen). cDNA was made using SuperScript III Reverse Transcriptase (Invitrogen). The V β 8-C β region was amplified using specific V β 8 (5'-ATTATTCATATGGTGCTGGC-3') and C β (5'-CGATCTTGGGTGGAGTCACATTTCTC-3') primers with required specific Ion Torrent tags. Purified PCR products were sent for high-throughput sequencing using the Ion Torrent platform. Sequence analysis was done with in-house software, and gene identity was assigned on the basis of sequence alignment with published sequences (International ImMunoGeneTics Information System). Alternatively, the exon 2 of CD1d genes was amplified by PCR with Phusion high fidelity polymerase (NEB) using specific primers (Forward primer 5'-TACACCTTCCGCTGCCT-3' and Reverse Primer 5'-AGCTACTCGATAGACTTGAAAC-3') with required specific Ion Torrent tags. Gel purified PCR products were sequenced with the Ion Torrent platform. Sequence analysis was done with in-house software, and gene identity was assigned on the basis of sequence alignment with published sequences.

Quantitative PCR. Total mRNA was extracted from sorted cells using TRIzol solution (Invitrogen, Carlsbad, CA). RNA was treated with the DNA-free kit (Ambion, Austin, TX) to remove contaminating DNA from RNA preparations. Reverse transcription was carried out by using the SuperScript III Kit (Invitrogen) following the manufacturer's instructions. The amount of amplicon generated during the PCR was monitored with a DNA engine Opticon 2 apparatus (MJ Research, Waltham, MA) by using gene specific primers and probes and the Platinum Quantitative PCR SuperMix UDG (Invitrogen). The sequences of the primers and probes are as follows: V α 14 forward 5-TACAGTGTGACCCCGACAAC-3, C α F 5-CCTCTGCCTGTTACCGACTT-3, C α R 5-TGGCGTTGGTCTCTTTGAAG-3, C α probe 5 FAM-CTCCCAAATCAATGTGCCGAAAACCA-TAMRA-

3; V α 14 probe 5 FAM-CACCCTGCTGGATGACACTGCCAC-TAMRA-3, J α 18 probe 5 FAM-AGCTGGGACTCAGCTGATTGTCATACCTG-TAMRA-3.

Flow Cytometry. PBS57-CD1d1 tetramer was obtained from the National Institutes of Health Tetramer Core Facility. The complete list of surface antibodies used is as follows: From BD Biosciences: anti-TCR β (H57-597), anti-CD8 α (53-6.7); From BioLegend: mCD1d (1B1), CD44 (IM7); From eBioscience: anti-B220 (RA3-6B2), anti-MHCII (I-A/I-E) (M5/114.15.2), anti-CD4 (RM4-5), anti-NK1.1 (PK1316). Surface antibody staining was done then cells were fixed and permeabilized using the FoxP3 buffer set (eBioscience). Fixed and permeabilized cells were incubated with intracellular antibodies including anti-PLZF (Mags.21F7; eBioscience), anti-Tbet (4B10; BioLegend), anti-ROR γ t (Q31-378; BD Biosciences), or anti-IFN γ (XMG1.2, eBioscience). Cells were analyzed on a BD LSRFortessa (BD Biosciences) and data were processed with FlowJo software (TreeStar).

Enrichment of CD1d reactive thymocytes. Thymocytes were enriched for PBS57-CD1d reactive cells by incubating thymocyte cell suspensions with PE or APC conjugated PBS57-CD1d tetramers for 45 minutes at 4°C, then incubated with anti-PE or anti-APC magnetic microbeads (Miltenyi Biotec) for 15 minutes at 4°C, followed by separation by using an autoMACS Pro Separator (Miltenyi Biotec) according to manufacturer's instructions. Cells were then later surface stained and then intracellular stained for flow cytometry.

***In vivo* iNKT cell stimulation.** Mice were administered vehicle or 2 μ g α GC (Funakoshi) by intravenous injection. Organs (spleen or liver) were harvested 90 minutes post injection. Cells were then later surface stained and then intracellular stained for flow cytometry without the use of brefeldin A or further activation. Mice were administered PBS or 40 μ g LPS (Sigma) by intravenous injection. Livers were harvested 7 hours post injection. Cells were surface stained and then intracellular stained for flow cytometry.

TCR β libraries preparation and T cell hybridoma. The 58 α ⁻ β ⁻ hybridoma cell line (65) was infected with hCD4-pA-GFP-NFAT-RV (66) and then cells positive for human CD4 were sorted using an Aria cell sorter 2d after transduction. Cells were next transduced with V α 14 iNKT TCR α chain-IRES-NGFR retrovirus and cells positive for NGFR were sorted. V β 8⁺ TCR rearrangements were amplified from total iNKT cells purified from the thymus of B6 or CD1D1^{-/-} mice and cloned into retroviral plasmids, as previously described (8). Cells were transduced with the retroviral TCR β libraries and TCR β ⁺ cells were sorted to obtain TCR α β ⁺ cells. TCR-reconstituted hybridomas (2.5 \times 10⁴ cells) were cultured for

18 h with antigens and CHB (5×10^5 cells) in 96-well round-bottomed plates. GFP expression on the hybridomas was analyzed by flow cytometry.

CHB transfectants. cDNA encoding CD1d1 and CD1d2 molecules were amplified from B6 or *CD1D1*^{-/-} splenocytes using the following primers 5'-ATTTATCTCGAGCCACCATGCGGTACCTACC-3' and 5'-ATTAAGAATTCTCACCGGATGTCTTGATAAGCGC-3' and cloned into retroviral plasmids. Plasmids were sequence verified and retroviruses were prepared as previously described (8) and used to transduce CD1d-negative CHB B cell lymphoma (67). Stably transduced cells were sorted for similar CD1d cell surface expression by flow cytometry using an Aria cell sorter (BD Bioscience). The C168W CD1D1 mutant was generated using QuikChange II Site-Directed Mutagenesis Kit following manufacturer's instruction. CHB cells expressing the C168W mutant were generated similarly.

Cloning, expression and purification of CD1d2. The mouse CD1d2/β2m gene harboring BirA and 6X-histidine tags was cloned into the baculovirus pFastBacDual expression vector as previously described (68). The CD1d2/β2m glycoprotein was expressed for 72 hours at 23°C using the High Five™ expression insect cells. The baculovirus-expressed soluble CD1d2/β2m protein was then concentrated, buffer exchanged against 20 mM Tris pH 8.5, 500 mM and purified by Ni-NTA. The protein was then dialyzed against 20mM Tris pH 8.5, 150 mM NaCl and further purified by size exclusion chromatography.

Crystallization and structure determination of CD1d2. The purified CD1d2 protein and CD1d2-αGC (C10) complex (8-10 mg/ml) in 20mM Tris pH 8.5, 150 mM NaCl was crystallized in 26% PEG 3350, 0.1 M Bis-Tris pH 6, 0.2 M CaCl₂ at 20°C using the hanging drop vapor diffusion method. The crystals were flash frozen prior to data collection in mother liquor containing 10-15% glycerol as a cryoprotectant. The crystals of CD1d2 were diffracted at the Australian Synchrotron facility (Melbourne). The dataset were processed and scaled using the programs iMosflm and SCALA from the CCP4 suite, respectively (69–71). The crystals diffracted to 2.3 Å resolution and belonged to the space group of P2₁ with two molecules in asymmetric unit. The crystal structures of CD1d2 and CD1d2-αGC(C10) were determined by molecular replacement using the Phaser-MR program (72) using the mouse CD1d1 as search model (PDB code: 1CD1) (45). The model building and subsequent refinement cycles were performed with the program COOT (73) and the refinement program BUSTER 2.10 (G. Bricogne *et al.* BUSTER version 2.10 Cambridge, United Kingdom: Global Phasing Ltd.; 2011), respectively. The quality of the final structure was validated using the PDB validation server from the PDB database (<https://validate-rcsb-1.wwpdb.org/>).

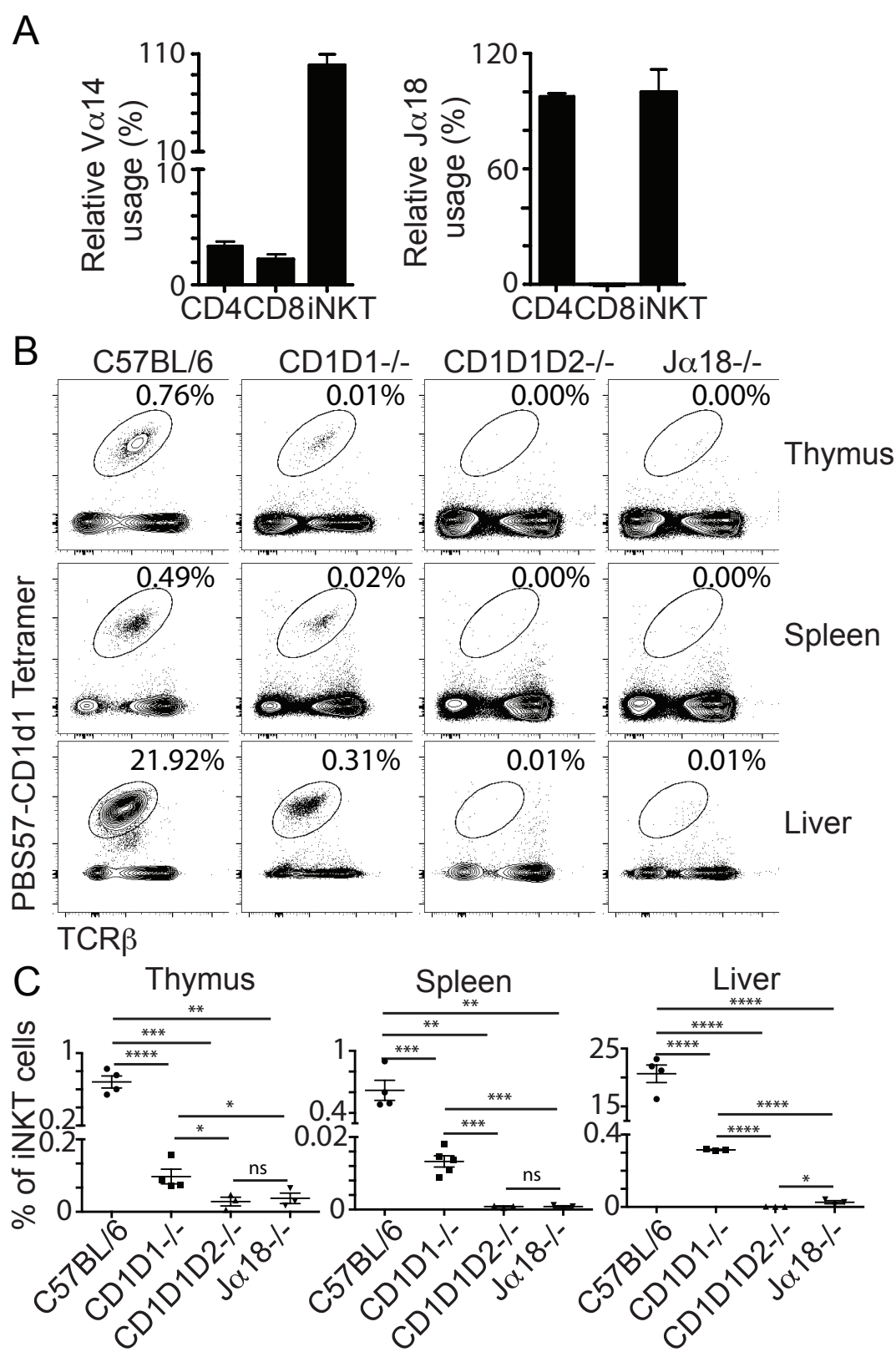
Biotinylation of CD1d2. For the purpose of biotinylation, the purified CD1d2 was desalted and incubated 8 parts of CD1d2 with 1 part of buffer A (100mM Bicine pH-8.3) and 1 part of buffer B (100 mM ATP, 100 mM MgOAc, 500 μ M D-biotin) along with 2 μ L of biotin protein ligase (1mg/mL). The biotinylation reaction was carried out at room temperature for overnight. The excess of free biotin was removed by size exclusion chromatography using superdex 200 10/30 gel filtration column.

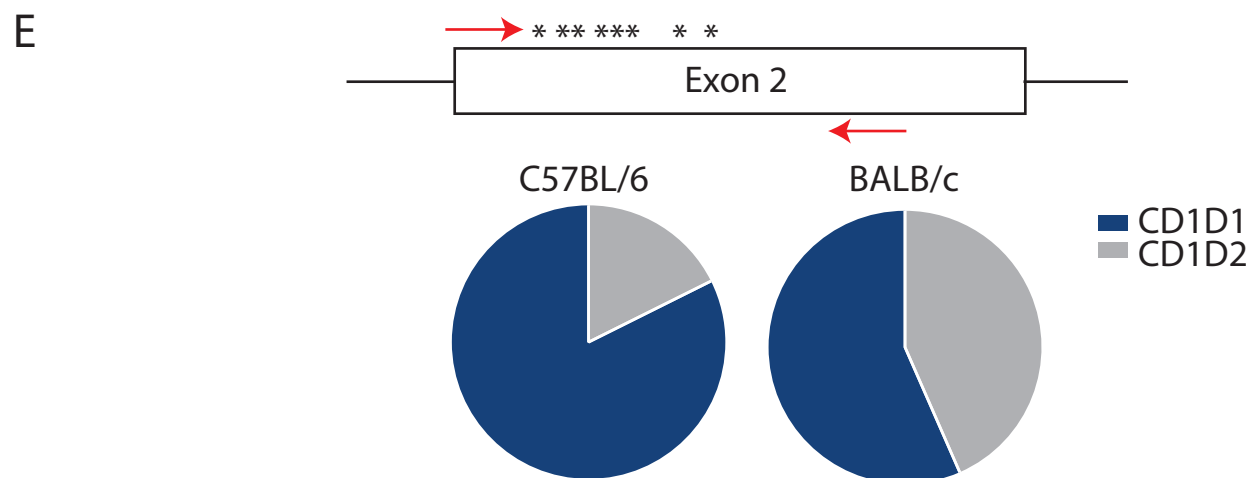
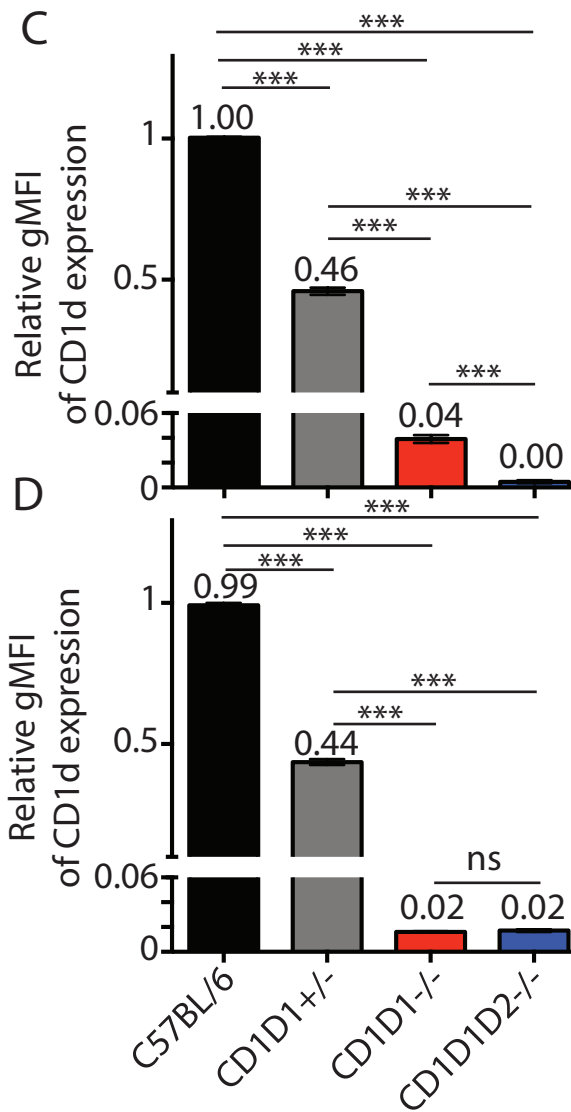
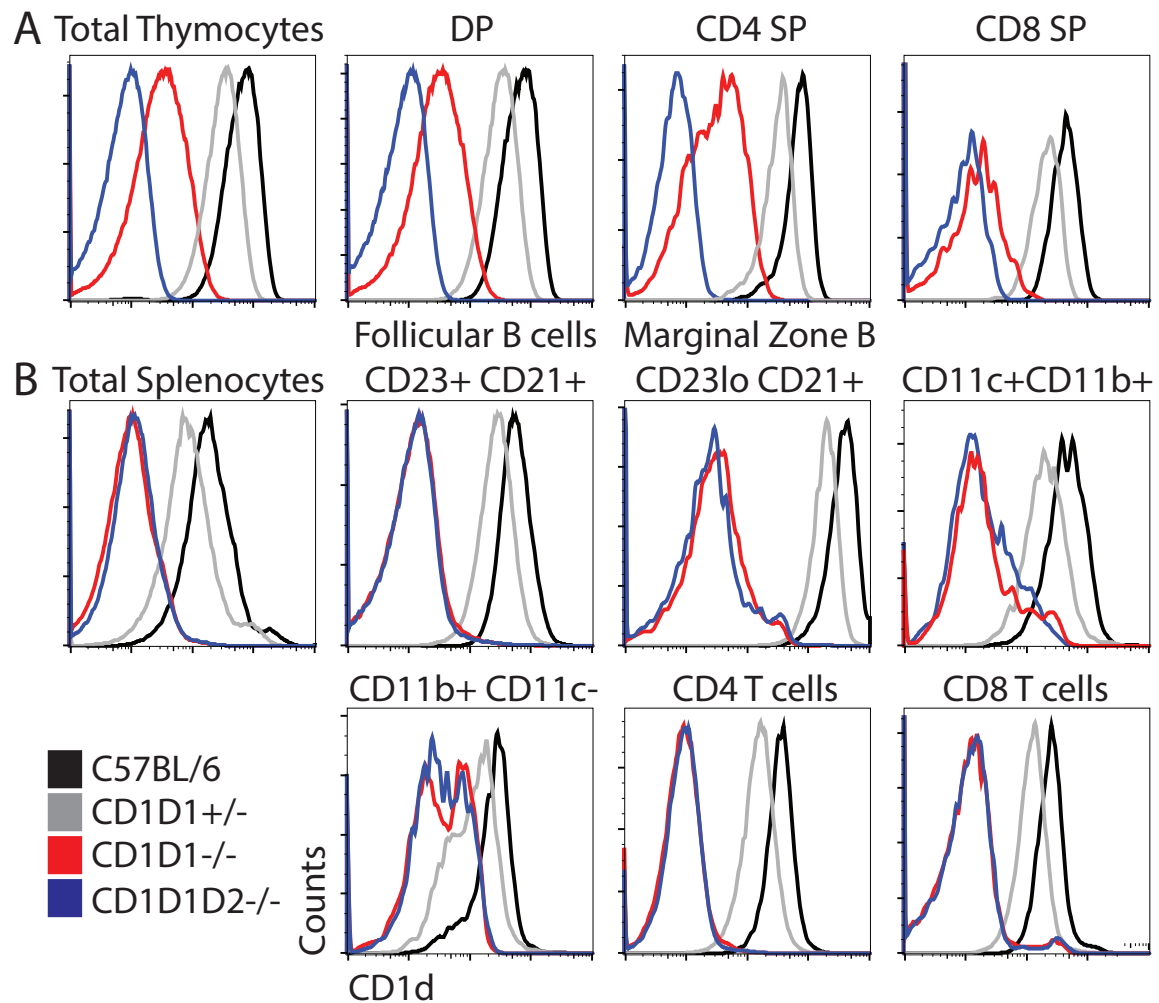
References

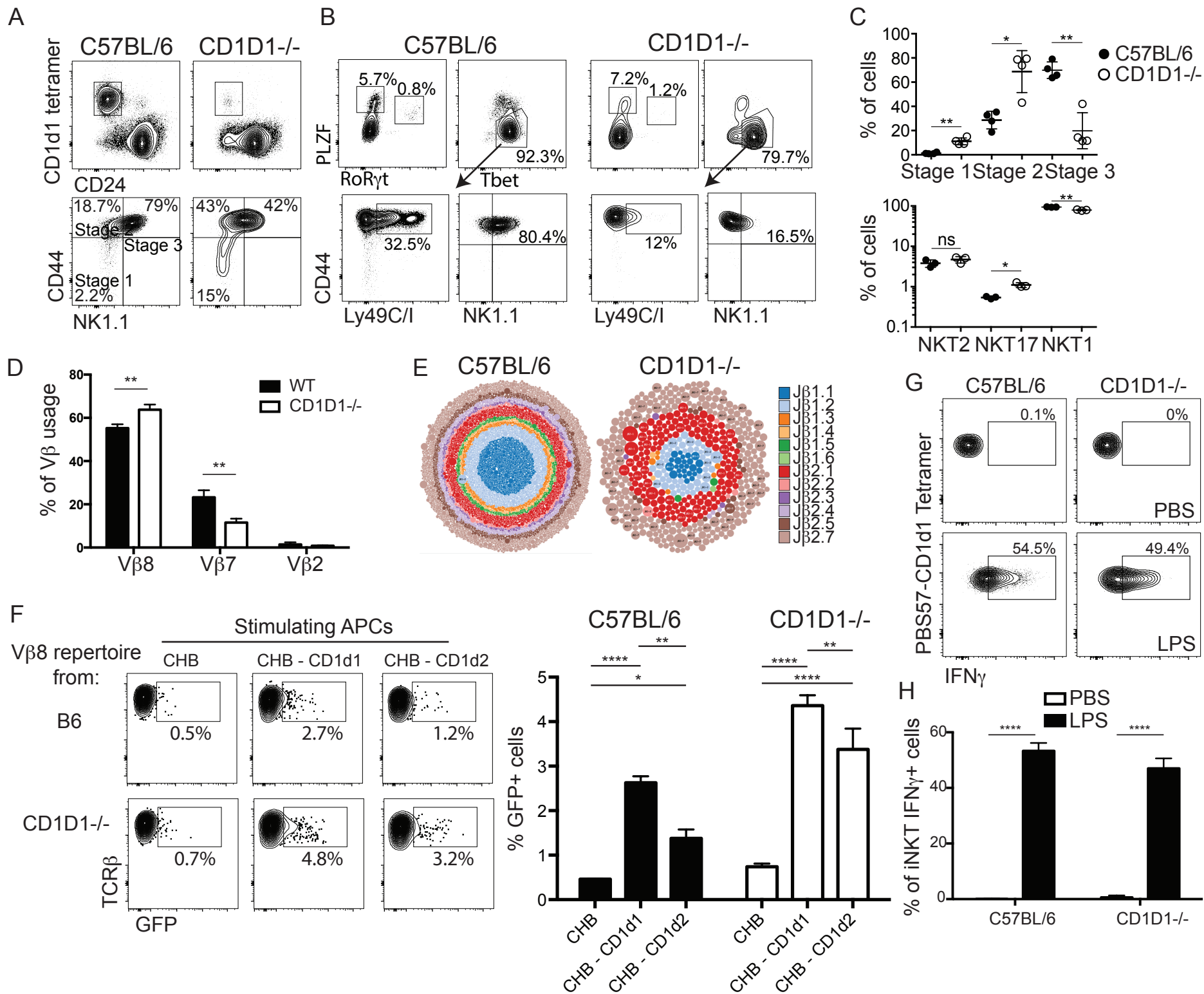
1. Adams EJ, Luoma AM (2013) The adaptable major histocompatibility complex (MHC) fold: structure and function of nonclassical and MHC class I-like molecules. *Annu Rev Immunol* 31:529–561.
2. Zajonc DM (2016) The CD1 family: serving lipid antigens to T cells since the Mesozoic era. *Immunogenetics* 68(8):561–576.
3. Van Rhijn I, Godfrey DI, Rossjohn J, Moody DB (2015) Lipid and small-molecule display by CD1 and MR1. *Nat Rev Immunol* 15(10):643–654.
4. Godfrey DI, MacDonald HR, Kronenberg M, Smyth MJ, Van Kaer L (2004) NKT cells: what's in a name? *Nat Rev Immunol* 4(3):231–237.
5. Lantz O (1994) An invariant T cell receptor alpha chain is used by a unique subset of major histocompatibility complex class I-specific CD4+ and CD4-8- T cells in mice and humans. *Journal of Experimental Medicine* 180(3):1097–1106.
6. Koseki H *et al.* (1990) Homogenous junctional sequence of the V14+ T-cell antigen receptor alpha chain expanded in unprimed mice. *Proceedings of the National Academy of Sciences* 87(14):5248–5252.
7. Rossjohn J, Pellicci DG, Patel O, Gapin L, Godfrey DI (2012) Recognition of CD1d-restricted antigens by natural killer T cells. *Nat Rev Immunol* 12(12):845–857.
8. Mallevaey T *et al.* (2009) T cell receptor CDR2 beta and CDR3 beta loops collaborate functionally to shape the iNKT cell repertoire. *Immunity* 31(1):60–71.
9. Pellicci DG *et al.* (2009) Differential recognition of CD1d-alpha-galactosyl ceramide by the V beta 8.2 and V beta 7 semi-invariant NKT T cell receptors. *Immunity* 31(1):47–59.
10. Patel O *et al.* (2011) Vbeta2 natural killer T cell antigen receptor-mediated recognition of CD1d-glycolipid antigen. *Proc Natl Acad Sci U S A* 108(47):19007–19012.
11. Matsuda JL, Mallevaey T, Scott-Browne J, Gapin L (2008) CD1d-restricted iNKT cells, the 'Swiss-Army knife' of the immune system. *Curr Opin Immunol* 20(3):358–368.
12. Brennan PJ, Brigl M, Brenner MB (2013) Invariant natural killer T cells: an innate activation scheme linked to diverse effector functions. *Nat Rev Immunol* 13(2):101–117.
13. Brigl M *et al.* (2011) Innate and cytokine-driven signals, rather than microbial antigens, dominate in natural killer T cell activation during microbial infection. *J Exp Med* 208(6):1163–1177.
14. Gapin L (2010) iNKT cell autoreactivity: what is 'self' and how is it recognized? *Nat Rev Immunol* 10(4):272–277.
15. Gapin L, Godfrey DI, Rossjohn J (2013) Natural Killer T cell obsession with self-antigens. *Curr Opin Immunol* 25(2):168–173.
16. Lee YJ, Holzapfel KL, Zhu J, Jameson SC, Hogquist KA (2013) Steady-state production of IL-4 modulates immunity in mouse strains and is determined by lineage diversity of iNKT cells. *Nat Immunol* 14(11):1146–1154.
17. Lee YJ *et al.* (2015) Tissue-Specific Distribution of iNKT Cells Impacts Their Cytokine Response. *Immunity* 43(3):566–578.
18. Crosby CM, Kronenberg M (2016) Invariant natural killer T cells: front line fighters in the war against pathogenic microbes. *Immunogenetics* 68(8):639–648.
19. Bradbury A, Belt KT, Neri TM, Milstein C, Calabi F (1988) Mouse CD1 is distinct from and co-exists with TL in the same thymus. *EMBO J* 7(10):3081–3086.
20. Dascher CC, Brenner MB (2003) Evolutionary constraints on CD1 structure: insights from comparative genomic analysis. *Trends Immunol* 24(8):412–418.
21. Brossay L *et al.* (1997) Mouse CD1 is mainly expressed on hemopoietic-derived cells. *J Immunol* 159(3):1216–1224.
22. Park SH, Roark JH, Bendelac A (1998) Tissue-specific recognition of mouse CD1 molecules. *J Immunol* 160(7):3128–3134.
23. Porcelli SA (1995) The CD1 family: a third lineage of antigen-presenting molecules. *Adv Immunol* 59:1–98.
24. Bjorkman PJ *et al.* (1987) Structure of the human class I histocompatibility antigen, HLA-A2.

- Nature* 329(6139):506–512.
25. Warburton RJ *et al.* (1994) Mutation of the alpha 2 domain disulfide bridge of the class I molecule HLA-A*0201. Effect on maturation and peptide presentation. *Hum Immunol* 39(4):261–271.
 26. Bendelac A (1995) Positive selection of mouse NK1+ T cells by CD1-expressing cortical thymocytes. *J Exp Med* 182(6):2091–2096.
 27. Chen Y-H, Chiu NM, Mandal M, Wang N, Wang C-R (1997) Impaired NK1+ T Cell Development and Early IL-4 Production in CD1-Deficient Mice. *Immunity* 6(4):459–467.
 28. Smiley ST, Kaplan MH, Grusby MJ (1997) Immunoglobulin E production in the absence of interleukin-4-secreting CD1-dependent cells. *Science* 275(5302):977–9.
 29. Mendiratta SK *et al.* (1997) CD1d1 Mutant Mice Are Deficient in Natural T Cells That Promptly Produce IL-4. *Immunity* 6(4):469–477.
 30. Chen YH *et al.* (1999) Expression of CD1d2 on thymocytes is not sufficient for the development of NK T cells in CD1d1-deficient mice. *J Immunol* 162(8):4560–4566.
 31. Hager E, Hawwari A, Matsuda JL, Krangel MS, Gapin L (2007) Multiple constraints at the level of TCRalpha rearrangement impact Valpha14i NKT cell development. *J Immunol* 179(4):2228–2234.
 32. Bedel R *et al.* (2012) Lower TCR repertoire diversity in Traj18-deficient mice. *Nat Immunol* 13(8):705–706.
 33. Kawano T *et al.* (1997) CD1d-restricted and TCR-mediated activation of V α 14 NKT cells by glycosylceramides. *Science* 278(5343):1626–1629.
 34. Zhang J *et al.* (2016) Mutation of the Traj18 gene segment using TALENs to generate Natural Killer T cell deficient mice. *Sci Rep* 6:27375.
 35. Uldrich AP *et al.* (2011) A semi-invariant Valpha10+ T cell antigen receptor defines a population of natural killer T cells with distinct glycolipid antigen-recognition properties. *Nat Immunol* 12(7):616–623.
 36. Lykke-Andersen S, Jensen TH (2015) Nonsense-mediated mRNA decay: an intricate machinery that shapes transcriptomes. *Nat Rev Mol Cell Biol* 16(11):665–677.
 37. Benlagha K, Kyin T, Beavis A, Teyton L, Bendelac A (2002) A thymic precursor to the NK T cell lineage. *Science* 296(5567):553–555.
 38. Pellicci DG *et al.* (2002) A natural killer T (NKT) cell developmental pathway involving a thymus-dependent NK1.1(-)CD4(+) CD1d-dependent precursor stage. *J Exp Med* 195(7):835–844.
 39. Gapin L (2016) Development of invariant natural killer T cells. *Curr Opin Immunol* 39:68–74.
 40. Benlagha K, Weiss A, Beavis A, Teyton L, Bendelac A (2000) In vivo identification of glycolipid antigen-specific T cells using fluorescent CD1d tetramers. *J Exp Med* 191(11):1895–1903.
 41. Matsuda JL *et al.* (2000) Tracking the response of natural killer T cells to a glycolipid antigen using CD1d tetramers. *Journal of Experimental Medicine* 192(5):741–754.
 42. Matsuda JL *et al.* (2001) Natural killer T cells reactive to a single glycolipid exhibit a highly diverse T cell receptor β repertoire and small clone size. *Proc Natl Acad Sci U S A* 98(22):12636–12641.
 43. Nagarajan NA, Kronenberg M (2007) Invariant NKT cells amplify the innate immune response to lipopolysaccharide. *J Immunol* 178(5):2706–2713.
 44. Vahl JC *et al.* (2013) NKT cell-TCR expression activates conventional T cells in vivo, but is largely dispensable for mature NKT cell biology. *PLoS Biol* 11(6):e1001589.
 45. Zeng Z *et al.* (1997) Crystal structure of mouse CD1: An MHC-like fold with a large hydrophobic binding groove. *Science* 277:339–345.
 46. Gadola SD *et al.* (2002) Structure of human CD1b with bound ligands at 2.3 Å, a maze for alkyl chains. *Nat Immunol* 3(8):721–726.
 47. Zajonc DM, Elsliger MA, Teyton L, Wilson IA (2003) Crystal structure of CD1a in complex with a sulfatide self antigen at a resolution of 2.15 Å. *Nat Immunol* 4(8):808–815.
 48. Scharf L *et al.* (2010) The 2.5 Å structure of CD1c in complex with a mycobacterial lipid reveals an open groove ideally suited for diverse antigen presentation. *Immunity* 33(6):853–862.
 49. Kain L *et al.* (2014) The identification of the endogenous ligands of natural killer T cells reveals

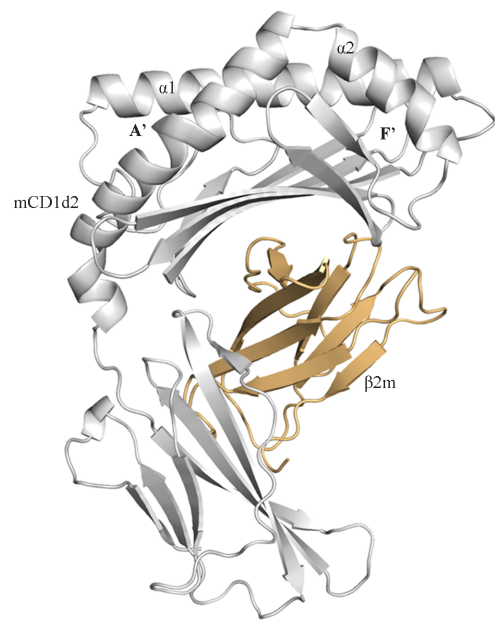
- the presence of mammalian alpha-linked glycosylceramides. *Immunity* 41(4):543–554.
50. Deng S *et al.* (2017) Psychosine variants as antigens for natural killer T cells. *Chem Sci* 8(3):2204–2208.
 51. Hughes AL, Hughes MK (1995) Natural selection on the peptide-binding regions of major histocompatibility complex molecules. *Immunogenetics* 42(4):233–243.
 52. Godfrey DI, Uldrich AP, McCluskey J, Rossjohn J, Moody DB (2015) The burgeoning family of unconventional T cells. *Nat Immunol* 16(11):1114–1123.
 53. Reinink P, Van Rhijn I (2016) Mammalian CD1 and MR1 genes. *Immunogenetics* 68(8):515–523.
 54. Schümann J, Mycko MP, Dellabona P, Casorati G, MacDonald HR (2006) Cutting edge: influence of the TCR Vbeta domain on the selection of semi-invariant NKT cells by endogenous ligands. *J Immunol* 176(4):2064–2068.
 55. Wei DG, Curran SA, Savage PB, Teyton L, Bendelac A (2006) Mechanisms imposing the Vbeta bias of Valpha14 natural killer T cells and consequences for microbial glycolipid recognition. *J Exp Med* 203(5):1197–1207.
 56. Birkinshaw RW *et al.* (2015) alphabeta T cell antigen receptor recognition of CD1a presenting self lipid ligands. *Nat Immunol* 16(3):258–266.
 57. Zajonc DM, Striegl H, Dascher CC, Wilson IA (2008) The crystal structure of avian CD1 reveals a smaller, more primordial antigen-binding pocket compared to mammalian CD1. *Proc Natl Acad Sci U S A* 105(46):17925–17930.
 58. Wang J *et al.* (2012) Crystal structures of bovine CD1d reveal altered alphaGalCer presentation and a restricted A' pocket unable to bind long-chain glycolipids. *PLoS One* 7(10):e47989.
 59. Wun KS *et al.* (2011) A molecular basis for the exquisite CD1d-restricted antigen specificity and functional responses of natural killer T cells. *Immunity* 34(3):327–339.
 60. Wang J *et al.* (2010) Lipid binding orientation within CD1d affects recognition of *Borrelia burgdorferi* antigens by NKT cells. *Proc Natl Acad Sci U S A*
 61. Rossjohn J *et al.* (2015) T cell antigen receptor recognition of antigen-presenting molecules. *Annu Rev Immunol* 33:169–200.
 62. Giabbai B *et al.* (2005) Crystal structure of mouse CD1d bound to the self ligand phosphatidylcholine: a molecular basis for NKT cell activation. *J Immunol* 175(2):977–984.
 63. Sievers F *et al.* (2011) Fast, scalable generation of high-quality protein multiple sequence alignments using Clustal Omega. *Mol Syst Biol* 7:539.
 64. Robert X, Gouet P (2014) Deciphering key features in protein structures with the new ENDscript server. *Nucleic Acids Res* 42(Web Server issue):W320–4.
 65. Letourneur F, Malissen B (1989) Derivation of a T cell hybridoma variant deprived of functional T cell receptor alpha and beta chain transcripts reveals a nonfunctional alpha-mRNA of BW5147 origin. *Eur J Immunol* 19(12):2269–2274.
 66. Ise W *et al.* (2010) CTLA-4 suppresses the pathogenicity of self antigen-specific T cells by cell-intrinsic and cell-extrinsic mechanisms. *Nat Immunol* 11(2):129–135.
 67. Haughton G, Arnold LW, Bishop GA, Mercolino TJ (1986) The CH series of murine B cell lymphomas: neoplastic analogues of Ly-1+ normal B cells. *Immunol Rev* 93:35–51.
 68. Patel O *et al.* (2011) NKT TCR recognition of CD1d-alpha-C-galactosylceramide. *J Immunol* 187(9):4705–4713.
 69. Winn MD *et al.* (2011) Overview of the CCP4 suite and current developments. *Acta Crystallogr D Biol Crystallogr* 67(Pt 4):235–242.
 70. Batty TG, Kontogiannis L, Johnson O, Powell HR, Leslie AG (2011) iMOSFLM: a new graphical interface for diffraction-image processing with MOSFLM. *Acta Crystallogr D Biol Crystallogr* 67(Pt 4):271–281.
 71. Evans P (2006) Scaling and assessment of data quality. *Acta Crystallogr D Biol Crystallogr* 62(Pt 1):72–82.
 72. McCoy AJ (2007) Solving structures of protein complexes by molecular replacement with Phaser. *Acta Crystallogr D Biol Crystallogr* 63(Pt 1):32–41.
 73. Emsley P, Lohkamp B, Scott WG, Cowtan K (2010) Features and development of Coot. *Acta Crystallogr D Biol Crystallogr* 66(Pt 4):486–501.



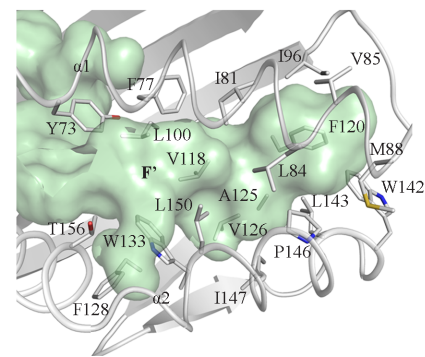
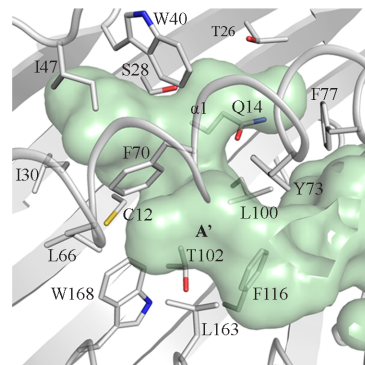




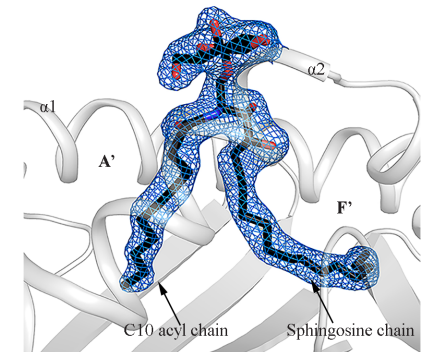
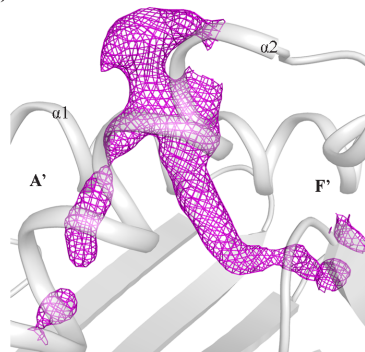
A)



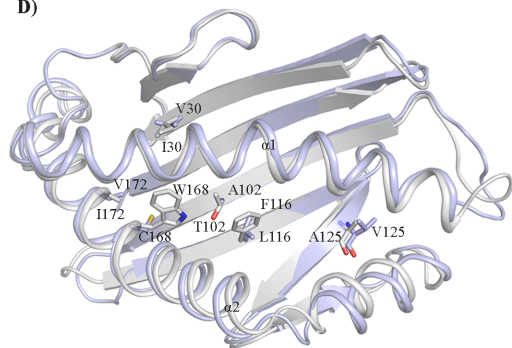
B)



C)



D)



E)

